HHS Public Access

Author manuscript

J Mater Chem B Mater Biol Med. Author manuscript; available in PMC 2016 June 14.

Published in final edited form as:

J Mater Chem B Mater Biol Med. 2015 December 14; 3(46): 8973–8982. doi:10.1039/C5TB01081K.

Effects of Silicon on Osteoclast Cell Mediated Degradation, *In Vivo* Osteogenesis and Vasculogenesis of Brushite Cement

Sahar Vahabzadeh, **Mangal Roy**, and **Susmita Bose***

W. M. Keck Biomedical Materials Research Laboratory, School of Mechanical and Materials Engineering, Washington State University, Pullman, WA 99164, USA

Abstract

Calcium phosphate cements (CPCs) are being widely used for treating small scale bone defects. Among the various CPCs, brushite (dicalcium phosphate dihydrate, DCPD) cement is widely used due to its superior solubility and ability to form new bone. In the present study, we have studied the physical, mechanical, osteoclast-like-cells differentiation and *in vivo* osteogenic and vasculogenic properties of silicon (Si) doped brushite cements. Addition of Si did not alter the phase composition of final product and regardless of Si level, all samples included β-tricalcium phosphate (β-TCP) and DCPD. 1.1 wt. % Si addition increased the compressive strength of undoped brushite cement from 4.78±0.21 MPa to 5.53±0.53 MPa, significantly. Cellular activity was studied using receptor activator of nuclear factor κβ ligand (RANKL) supplemented osteoclast-like-cells precursor RAW 264.7 cell. Phenotypic expressions of the cells confirmed successful differentiation of RAW264.7 monocytes to osteoclast-like-cells on undoped and doped brushite cements. An increased activity of osteoclast-like cells was noticed due to Si doping in the brushite cement. An excellent new bone formation was found in all cement compositions, with significant increase in Si doped brushite samples as early as 4 weeks post implantation in rat femoral model. After 4 weeks of implantation, no significant difference was found in blood vessel formation between the undoped and doped cements, however, a significant increase in vasculgenesis was found in 0.8 and 1.1 wt. % Si doped brushite cements after 8 weeks. These results show the influence of Si dopant on physical, mechanical, *in vitro* osteoclastogenesis and *in vivo* osteogenic and vasculogenic properties of brushite cements.

Keywords

Brushite cement; Si doping; *in vitro* osteoclastogenesis; TRAP assay; *in vivo* osteogenesis; *in vivo* vasculogenesis

1. Introduction

In the class of calcium phosphate bone substitutes, calcium phosphate cements (CPCs) have unique self-setting property at body temperature, high mouldability with adequate biocompatibility and degradation rate [1,2,3]. One of the first orthopedic CPCs was formulated by Brown and Chow in 1986 [4]. Since then, several reports have been published

*Corresponding Author: Tel: 509 3357461; Fax: 509 3354662; sbose@wsu.edu.

on CPCs' potential applications in bone defect filling, osteosynthetic screw reinforcement, pulp tissue engineering, and drug delivery [2,5,6].

There are two major classes of CPCs based on the final product of cement reaction; 1) apatitic cement in which hydroxyapatite (HA, $Ca_{10}(PO_4)_6(OH)_2$) or calcium deficient HA (CDHA, $Ca_{10-x}(HPO_4)_x(PO_4)_{6-x}(OH)_{2-x}$) is formed and 2) brushitic cement which contains brushite (dicalcium phosphate dihydrate, DCPD, $CaHPO_4.2H_2O$) as the final product [6]. Formation of either of above phases depends on the initial chemistry of the cement paste [7,8]. Among these two cements, solubility product (Log K_{sp}) of DCPD and HA is −6.6 and −117.1, respectively at 25ºC [8,9], resulting in higher chemical dissolution of brushite cements [10,11,12]. Along with chemical degradation, cell mediated resorption plays an important role in degradation of brushite cement and its overall bone regeneration capability, that is in dynamic equilibrium between bone forming osteoblast cells and bone resorbing osteoclast cells [13,14]. Consequently, to examine the validity of a biomaterial towards bone tissue engineering application, not only the osteoblast, but also the osteoclast cellular activity should be studied. We hypothesize that the chemistry of brushite cement plays a crucial role in its interaction with osteoclast cells.

It is well documented that bioactivity of brushite can be further enhanced by several cement modifications [3, 15–19]. Zinc (Zn) and strontium (Sr) substitutions in brushite cements (BrCs) not only enhance alkaline phosphatase (ALP) activity, but also stimulate preosteoblastic proliferation and type-I collagen secretion in comparison to pure cement [3]. Magnesium (Mg) substituted brushite cements show improvement in mechanical properties, increased setting time, and enhanced osteoblast cell proliferation and differentiation [15]. Silicate addition as a bioactive component to the mixture of tricalcium phosphate (TCP)/ monocalcium phosphate monohydrate (MCPM) improves injectability of cement and bioactivity, stimulates bone marrow stromal cells (BMSCs) proliferation and promote osteoblastic differentiation of BMSCs [16,17,18,19]. In this work, we have focused our attention to show the effects of Si and its concentration on phase composition, compressive strength, setting time, dissolution behavior and *in vitro* osteoclastogenesis of BrCs.

Addition of trace elements is also known to alter the material- osteoclast cell interactions in CaPs. Recent literatures have reported the inhibitory effect of magnesium and zinc doping on osteoclast differentiation in β-TCP ceramics [20,21]. On the other hand, enhanced osteoclast activity is reported in Si incorporated HA ceramic [22]. Si, being an essential trace element for bone tissue development shows much promise in designing biomaterials for bone-tissue engineering through enhancement of bone apposition and vasculogenesis [16–19]. Vasculogenesis is important in tissue engineering, as new blood vessels provide oxygen and nutrients in tissue engineered constructs [23]. Therefore, we have studied the effects of Si and its concentration on not only the *in vitro* osteoclastogenesis, but also *in vivo* osteogenesis and vasculogenesis of BrCs using a rat distal femur model.

In view of the beneficial effects of Si, our objective of present study is to understand the effects of Si doping at different concentrations on physical, mechanical, osteoclastogenesis and *in vivo* osteogenesis and vasculogenesis of brushite cements. The influence of Si on osteoclastogenesis was studied *in vitro* using RAW 264.7 mononuclear cells supplemented

with receptor activator of nuclear factor κβ ligand (RANKL). It has been reported that RAW 264.7 mononuclear cells differentiate to osteoclast cells in presence of RANKL with no need for macrophage colony stimulating factor (M-CSF) [24].

Cell differentiation was confirmed by cellular morphology, tartrate resistant acid phosphatase (TRAP) assay, actin ring formation, and resoprtion was confirmed by pit formation. Moreover, the compositional dependence of osteogenesis and vasculogenesis in brushite cements was studied by histomorphology and histomorphometry at 4, 8, and 12 weeks post implantation in rat distal femoral model. To the best of our knowledge, there is no report on the effects of Si and its concentration on physical, mechanical, *in vitro* osteoclastogenesis and *in vivo* osteogenesis and vasculogenesis of brushite cements.

2. Materials and Methods

2.1. Cement preparation and characterization

The brushite cement was prepared as mentioned elsewhere [25]. Briefly, β-TCP and MCPM were mixed at a molar ration of 1:1. The final mixture of cement was composed of 42 wt. % fine β-TCP, 31 wt. % granular β-TCP, 21 wt. % MCPM, 5 wt. % magnesium hydrogen phosphate trihydrate, in addition to small amounts of magnesium sulphate and sodium hydrogen phosphate to modify the setting time [26,27]. 0.5, 0.8, and 1.1 wt. % Si-doped brushite cements were made by mixing relative amount of SiO_2 with precursors of β-TCP, followed by calcination of precursors at 1050 °C. The cement paste was prepared by mixing the BrC powder and 2 wt. % PEG solution at powder to liquid ratio (P/L) of 3.33:1 and then poured into a 6 mm diameter and 12 mm height mold. The polymer concentration and P/L ratio was selected based on our previous work [25]. Cements were kept under 100 % humidity condition for one hour, followed by immersion in PBS for 24 hour at 37 ºC.

From now on undoped, 0.5 wt. %, 0.8 wt. % and 1.1 wt. % Si-doped brushite cements will be denoted as BrC, 0.5 Si-BrC, 0.8 Si-BrC, and 1.1 Si-BrC, respectively. Phase analysis, compressive strength and setting times of undoped and doped BrCs were evaluated using X-ray diffractometer (XRD), screw-driven universal testing machine, and Gillmore needle as described in supporting data.

2.2. In vitro osteoclastogenesis

2.2.1. Osteoclast cell culture and characterization—Prior to cell culture, BrCs were sterilized using ethanol soaking followed by sterilization under UV for 30 minutes. The mouse monocyte cell line RAW 264.7 (ATCC, USA) was seeded at a density of 10^5 cells/sample. Dulbecco's Modified Eagle's Medium (DMEM, ATCC, Manassas, VA) supplemented with 10 vol. % fetal bovine serum (FBS, Sigma, St. Louis, MO) and 1 vol. % penicillin/streptomycin (Invitrogen, Germany) was added and samples were incubated in an atmosphere of 5 % CO_2 at 37°C. After 1 day, 50 ng/mL RANKL (Biolegend, CA) was added to the cell culture medium. Since this time point, RANKL supplemented cell culture medium was changed every 2–3 days for the rest of the experiment.

The morphology of osteoclast cells was studied using field emission scanning electron microscope (FESEM, FEI 200F, FEI, OR), as explained in supporting data.

Immunohistochemistry and confocal laser microscopy were also used to study the formation of osteoclast cells, as described in supporting data.

2.2.2. TRAP activity—TRAP activity was measured after 8 and 14 days of culture according to the protocol [20]. Briefly, adherent osteoclast-like-cells were lysed in 1 M NaCl containing 0.2 % Triton X-100. The lysate were then incubated for 30 min at 37 °C with 50 mL of 5 mM p-nitrophenyl phosphate (Sigma, USA) in 25 mM Na acetate–20 mM Na tartrate with pH 4.8. 0.5 M NaOH was added to stop the reaction. 150 μL of the resulting supernatant was transferred into a 96-well plate and read by a UV–Vis spectroscopy (BioTek) at 405 nm. Three samples were used for each composition at each time point and data were reported as mean ± standard deviation of three technical samples.

2.2.3. Resorption pit assay—To investigate the resorption pit morphology resulted from the osteoclast-like-cell activity, cells were detached from the sample surface after 8 and 14 days of culture. To remove the osteoclast-like-cells, samples were ultrasonicated in 1 M NaCl solution containing 0.2% Triton X-100, followed by rinsing with PBS. After gold coating, the resorption lacunae on BrCs were observed under FESEM.

2.3. In vivo study

In the present study, a total number of 18 male Sprague-Dawley rats (Simonsen Laboratories, Gilroy, CA, USA) with an average body weight of 300 g were used.

2.3.1. Surgery and implantation procedure—Surgeries were performed according to the Institutional Animal Care and Use Committee (IACUC) approved protocol in Washington State University. The rats were housed in individual cages with alternating 12-hour cycles of dark and light in humidity and temperature controlled rooms prior to surgery. Combination of IsoFlo® (isoflurane, USP, Abbott Laboratories, North Chicago, IL, USA) and oxygen (Oxygen USP, A-L Compressed Gases Inc., Spokane, WA, USA) was used during the anesthesia. After shaving and disinfection by povidone iodine 5%, a longitudinal skin incision was made in the distal region of the lateral aspect of the distal femur of all animals. Using a drill and at a slow rotation speed, a circular defect with size of 3 mm in diameter was created in the distal. Cement powders were mixed with PEG solution and were then implanted. Following implantation, muscle and skin were closed in layers using synthetic absorbable surgical suture (Ethicon Inc., Somerville, NJ, USA). To prevent infection, povidone iodine 5 % disinfectant was applied to the wound site. At 4, 8, and 12 weeks post-surgery, rats were euthanized by halothane overdosing, followed by an intracardiac injection of potassium chloride (70%).

2.3.2. Histomorphology—Implanted BrCs were fixed in 10 % buffered formalin solution for 72 h prior to histological analysis. The specimens were decalcified and then dehydrated for decalcified tissue sections preparation, and further used for Hematoxylin and eosin (H&E) and Von Willebrand Factor (vWF) staining.

2.3.2.1. Hematoxylin and eosin (H&E) staining: After fixation in buffered formalin solution, samples were kept in 14 % ethylenediaminetetraacetic acid (EDTA) until

demineralization. After demineralization, samples were dehydrated in ethanol series (30 %, 50 %, 70 %, 90 %, and 100 %), ethanol-xylene (1:1, two times), and 100% xylene (two times). Samples were then embedded in paraffin, and a microtome was used to cut them to 8 to 12 μm thick tissue sections. Then, the tissue sections were deparaffinized and used for H&E staining.

2.3.2.2. Von Willebrand Factor (vWF) staining: Samples were decalcified as described in 2.8.2.2. Deparaffinized slides were stained for vWF using a blood vessel staining kit (ECM590, Millipore, MA, USA). Briefly, rabbit anti-vWF polyclonal antibody was used as the primary antibody. Antigen retrieval was carried out by heating the slides in sodium citrate buffer (10mM sodium citrate, 0.05 % tween 20, pH 6.0) in a vegetable steamer for 20 min. Haematoxylin was used as the counterstain. The immunohistochemical stained sections were then dehydrated in ethanol series (70%, 95% and 100%), cleared in two changes of xylene, and mounted with Permount.

2.3.3. Histology—Image J software (National Institute of Health) was used for calculation of total bone formation (bone area/area of the entire tissue section, %) and blood vessel area (blood vessel area/total area, %) from Hematoxylin and Eosin (H&E), and blood vessel stained tissue sections, respectively.

2.4. Statistical analysis

Quantitative data for compressive strength, TRAP activity, total new bone area, and blood vessel area are expressed as mean ± standard deviation. Statistical analysis was performed using student's *t*-test, and P value < 0.05 was considered significant.

3. Results

3.1. Phase analysis, setting time and compressive strength

Figure 1a shows the XRD patterns of cements after 1 day incubation in PBS. DCPD (JCPDS no. 09-0077) and β-TCP (JCPDS no. 09-0169) were the only phases present in all samples and no other phases were found. Addition of Si in cements did not introduce any new phase.

Phase analysis of cements after 14 days of immersion in DMEM (without cell) is presented in Figure 1b. All samples included β-TCP and DCPD, and no other phase was present. Table 1 shows the ratio of peak heights of β-TCP (2θ~ 31.1°) and DCPD (2θ~ 21°) before and after immersion in DMEM. β-TCP/DCPD ratio increased for all samples, however, the highest increase was found for undoped BrC.

The effects of dopant incorporation on initial and final setting times of BrCs are presented in Table 1. Dopant introduction to BrCs decreased the initial setting times from 5 min to 3.5 min for undoped and 0.5 Si-BrCs, respectively. Initial setting time for 0.8 Si-BrC and 1.1 Si-BrC was 4 min. Final setting time for undoped, 0.5 Si-, and 0.8 Si-BrCs was 11–12 min; however, a significant increase in final setting time to 19 min was found for 1.1 Si-BrC.

Figure 2 represents the compressive strength of BrCs after 1 day incubation in PBS. Compressive strength of BrC, 0.5 Si-BrC, and 0.8 Si-BrC was 4.78±0.21 MPa, 4.49±0.54

MPa, and 4.85± 0.31, respectively. Addition of 0.5 and 0.8 wt. % Si did not alter the compressive strength significantly. However, incorporation of 1.1 wt. % Si resulted in significant increase in compressive strength to 5.53±0.53 MPa.

3.2. Osteoclast cell phenotype

As shown in Figure 3, monocytes adhered spontaneously to the cement samples through microextensions around their periphery after 5 days of culture. As the characteristic of RAW 264.7 cell, some of the monocytes had fused together to form giant osteoclast-like-cells on all of the cement samples. At this time point, effect of Si addition on monocyte attachment on cement samples was negligible. The monocyte fusion and giant osteoclast-like-cell formation continued up to day 8. Along with osteoclast-like-cell formation, monocytes proliferation was still ongoing on 0.5Si-BrC samples compared to undoped and other doped cement samples. At day 8, 0.8Si-BrC and 1.1Si-BrC also showed osteoclast-like-cell formation, however much less monocyte proliferation was found on these two samples.

Formation of osteoclast-like-cells on the undoped and Si doped cement samples were also confirmed by immunohistochemical analysis. Immunohistochemistry was used to prove the multinuclearity of cell, presence of vitronectin receptor $\alpha_v\beta_3$ and actin ring formation around the cells, as characteristics of osteoclast, after 8 and 14 days of culture. Figure 4a shows the confocal micrographs of RAW 264.7 cells cultured on BrCs for 8 days in RANKL supplemented media. After 8 days of culture, multinuclear cells with actin ring around the cell periphery and highly expressed $\alpha_v\beta_3$ integrin were observed on all types of cements. Correlating the SEM results.

0.5Si-BrC also showed higher monocytes at day 8 compared to undoped and other Si doped samples. Figure 4b shows the fluorescence microscope images of osteoclast-like-cells after 14 days of culture. Higher amount of multinuclear osteloclast-like-cells were found on 0.5Si-BrC sample at day 14. Large multinuclear osteoclast-like-cells were also found in BrC, 0.8Si-BrC, and 1.1Si-BrC samples; however, fewer than 0.5Si-BrC sample.

3.3. TRAP assay

Expression of TRAP, as a characteristic of osteoclasts, was evaluated at day 8 and 14. Figure 5 shows TRAP synthesis by osteoclast-like-cells as a function of cement composition and culture day. After 8 days of culture, expression of TRAP by osteoclast-like-cells was significantly higher on all doped BrCs and the highest amount was found for 0.5 Si-BrC. The TRAP assay results are in agreement with cell morphology and immunohistochemical analysis of osteoclast-like-cells on undoped and doped cement samples after 8 days of culture. After 14 days of culture, TRAP synthesis increased significantly for BrC, 0.5Si-BrC, and 0.8Si-BrC which indicated higher number of osteoclast-like-cell formation for these samples.

Surface resorption of cements due to osteoclast-like-cell activity was determined by removing the cells and observing surface morphology. Figure 6 shows the resorption lacunae on undoped and doped BrCs after 8 and 14 days of culture in RANKL supplemented media. Prominent resorption lacunae were noticed on all samples as early as day 8 of culture. The localized resorption lacunae with distinct borders around the pit indicated cell

mediated resorption. There was no obvious difference in size and shape of resorption pits on undoped and Si doped-BrCs. As osteolast-like-cells formed on both undoped and Si doped BrC samples on day 5, it is expected that resorption pit will form on all of the samples in a similar manner with little to no distinguishable features among them. At day 14 resorption pit depth increased in all samples indicating continual activity of the osteoclast-like-cells. The significant difference was noticed in 1.1 Si-BrC cement where the lacunae not only increased in depth, but also increased in size as well.

3.4. In vivo study; histomorphology and histomorphometric analysis

Bone formation was studied using H&E staining and the results are presented in Figure 7a. Acellular region derived from demineralization process of BrCs is seen in this Figure. This figure depicts a clear view of new bone formation in entire surgery site for all BrCs after 4 and 8 weeks. Samples harvested at 12 weeks showed a complete bone formation and the surgery site was not detectable due to complete degradation of cements. Figure 7b shows the histomorphometric analysis of new bone area calculated from H&E stained BrC sections. It shows that after 4 weeks, there was a significant increase in bone formation in 0.5 and 0.8 Si-BrCs. Although there was an increase in bone formation for 1.1Si-BrC compared to BrC, this increase was not significant. After 8 weeks the difference in new bone formation between undoped BrC and all doped BrCs was significant.

Figure 8a shows the blood vessel formation inside the BrCs after 4 and 8 weeks. New blood vessel was formed in all BrCs at both time points. Histomorphometric analysis of blood vessel staining is presented in Figure 8b. At 4 weeks, a significant decrease in blood vessel formation was seen in 0.5Si-BrC compared to BrC. However, higher amount of Si did not have adverse effect on blood vessel formation. At 8 weeks, there was no significant change in new blood vessel formation in undoped BrC compared to 4 weeks; however, there was a significant increase in blood vessel formation in all three doped samples compared to 4 weeks.

4. Discussion

Brushite cements have received significant attentions in bone regeneration application due to their bioactivity, osteoconductivity, and reasonable biodegradation rate. Although chemical degradation is one of the dominant mechanisms for brushite cement biodegradation, cell-mediated biodegradation can also play a significant role in overall bone remodeling [7,14]. In the present work, we primarily discuss the effects of Si addition on physical, mechanical, *in vitro* osteoclast cell interaction, and *in vivo* osteogenesis and angiogenesis properties of brushite cements.

Based on our previous work, cements are prepared by mixing cement powder with 2 wt. % PEG to form the paste and then incubating for one hour in 100 % humidity followed by soaking for 24 hours in PBS [25]. XRD results indicate that β-TCP and DCPD are the only two phases present in the final product. No other phases containing Si is formed which is due to the low amount of dopant.

Si addition did not affect the initial setting time; however, final setting time increased to 19 min with addition of 1.1 Si to BrC. Brushite setting reaction includes dissolution of cement component in solution, formation of supersaturated gel, and nucleation and growth of DCPD. In β-TCP /MCPM system, cement formation begins with MCPM dissolution where pH drops to 2.0–2.5, followed by β-TCP dissolution. Finally, DCPD precipitation occurs which results in a pH jump [28,29]. Presence of additives such as sulphate and pyrophosphate ions prolongs the setting reaction [27], which is desired as it gives enough time to mix the cement component before reaching the final setting. Although addition of Si at low levels does not change the final setting time of cement, addition of 1.1 wt% Si, increased the final setting time from 11–12 min to 19 min. This represents the retarding effect of Si on setting reaction in β-TCP/MCPM system. Si incorporation in calcium phosphates, i. e. β-TCP and HA, is accompanied by increase in dissolution rate of material [30,31]. As silica was mixed with β-TCP precursors in present work, the retard in setting reaction at higher Si level may be attributed to its inhibitory effect on DCPD precipitation and growth.

According to ASTM standard (ISO 5833), cements should be allowed to set at least for 24 hours, preferably under physiological condition for biomedical applications, before mechanical testing. In addition to main components of cement, ionic substitution and presence of polymer, alters the mechanical properties of cements [11,25]. Prolonged setting reaction that inhibits the cement crystal growth is directly related to increase in compressive strength [32]. Significant increase in final setting time due to presence of Si, retards the DCPD precipitation and growth, and increases the compressive strength of BrCs.

For bone regeneration application, the interaction between biomaterial and bone cells should be studied. Many reports present the effects of Si doping on HA and β-TCP interactions with osteoblast cells; however, few reports investigate the osteoclast cell interaction with Si doped calcium phosphates. FESEM images show attachment of RAW 264.7 monocytes to all samples via cellular microextensions. Adhesion of monocytes is an important step in osteoclast formation. In addition, similar type of attachment to substrate in all samples indicates that the amount of Si doping does not affect the monocyte adhesion. Adhered monocytes progressively differentiate into osteoclast-like-cells depending on material properties. In the present study, cells featuring osteoclast-like-cells are present in BrC, 0.5 Si-BrC, 0.8 Si-BrC, and 1.1 Si-BrC samples after 8 and 14 days of culture, indicating successful differentiation of RAW264.7 cells into osteoclast-like-cells. Cement composition is found to have minimal effect on osteoclast-like-cell morphology. However, quantitative assay shows that all Si doped BrCs have higher TRAP activity compared with undoped BrC which signifies that Si addition enhances osteoclastogenesis on doped BrCs. Presence of actin ring on periphery of multinuclear regions found by immunohistochemistry method also approves the presence of osteoclast cells on all samples after 8 and 14 days. From the TRAP assay results, it is evident that the optimum amount of Si addition is 0.5 wt. % for the highest osteoclast-like-cell differentiation which is also evident from 14 days results. Osteoclastogenesis development and resorption dependence on Si concentration has also been reported previously where lower concentrations (30ppm) of Si stimulated osteoclast response while higher concentrations inhibited osteoclast development and resorption [19]. Increase in osteoclast differentiation in Si-doped calcium phosphate is in line with other

works [22]. *Lehmann et al.* reports higher osteoclast activity in 1.4 wt% Si doped HA compared to undoped HA disk [33]. However, less bioactivity in high amount of Si is also reported in HA/α-TCP binary system [34]. Although several literature reports dose dependent effects of Si doping in HA/TCP towards osteoclast formation and resorption, to the best of our knowledge, no specific reason of osteoclastogenesis has been related to Si. Future work related to effects of Si on key gene expressions essential for osteoclastogenesis has to be done to have a better scientific understanding.

Si addition can alter β-TCP/DCPD ratio during immersion in cell media. It is well known that DCPD in brushite cement would be stable, dissolve or hydrolyze to HA, depending on environmental conditions [10,11]. XRD results revealed no peak related to HA in all BrC samples after immersion. This is due to hindrance effect of magnesium salt and pyrophosphate ion in present work on HA hydrolysis process. Magnesium ion in form of $MgHPO_4.3H_2O$ attaches to the surface of HA nuclei, blocks the growth site, and inhibits further HA crystallization. In addition, sodium pyrophosphate ($Na_2H_2P_2O_7$) acts as crystal growth obstacles [35,36]. As a result, less increase in β-TCP/DCPD ratio may be due to increase in β-TCP dissolution rate in doped samples. It is also known that solubility of β-TCP will increase with Si doping [31]. Therefore, higher amount of β-TCP has converted to DCPD for Si doped samples during 14 day immersion.

The effects of Si and its concentration on osteogenesic and vasculogenesis properties of BrC are investigated. Initiation of osteoid formation in host bone-cement interface is found in current work. Early mineralization of osteoid in Si doped BrCs shows the effective role of Si in biomineralization process (Figure 1S). Significant increase in total bone area after 4 and 8 weeks of implantation in all doped BrCs is shown in Figures 7a and b which is reported elsewhere [35]. Our results show that although the higher *in vitro* osteoclast activity is found in Si doped BrCs, the total bone formation is accelerated *in vivo*. Si substitution in HA scaffolds encourages the bone growth in rabbit model [37]. Si has stimulatory effect on proliferation, differentiation, and mineralization of osteoblast cells [38]. It upregulates the ALP activity in both osteoblasts and mesenchymal stem cells [39]. At early stages of biomineralization, Si is present in calcification sites and at later stages Si induces the precipitation of HA from electrolyte solution [19]. It has been suggested that early osteogenesis by silicon is caused by synthesis and/or stabilization of collagen [40]. However, the exact mechanism and possible signaling pathways need to be understood. Although higher bone formation is found in doped samples, there is no significant change between 4 and 8 weeks data. This is related to accelerated degradation of BrCs due high solubility product of DCPD and porous nature of BrC.

Vasculogenesis or new blood vessel formation is crucial in functional tissue-engineered constructs. Blood vessels carry the oxygen and nutrient supply to maintain the tissue function and overall survival. The results presented in Figures 8a and b show the dependency of blood vessel formation on dopant concentration. Significant increase in vasculogenesis in all doped BrCs at 8 weeks post implantation in comparison to 4 weeks proves the positive effect of Si and its concentration on vasculogenesis. Although the complete mechanism governing the blood vessel formation in calcium phosphates are yet to be understood, it has been shown that Si upregulates the nitric oxide synthase and increases

the VEGF production in bioglasses and calcium silicate materials in dose dependent manner through enhancement of vascular endothelial growth factor receptor (VEGFR-2) and basic fibroblast growth factor receptor (bFGF) in endothelial cells [41,42,43]. In addition, upregulation of endothelial gene markers by human dental pulp stromal cells (HDPSCs) shows the efficacy of bioglasses in regeneration of vascularized bone substitutes in combination of HDPSCs [44]. Increase in expression of VEGF is also reported in human umbilical vein endothelial cells (HUVEC) alone and co-cultured with human dermal fibroblasts (HDFs) due to Si ion release [45]. These results show the effects of Si amount on physical, mechanical, and *in vivo* osteogenic and vasculogenic properties of BrCs, which can be tailored to meet specific clinical application needs.

5. Conclusions

Here we report the effects of Si dopant addition on physical, mechanical, osteoclast differentiation, and *in vivo* osteogenic and vasculogenic properties of brushite cements. Addition of Si did not introduce any new phase in brushite cements; however, affected the cement formation and degradation kinetics. 1.1 wt. % Si addition increased the compressive strength of undoped brushite cement from 4.78±0.21 MPa to 5.53±0.53 MPa, significantly. A dose dependent effect of Si doping on osteoclast cell differentiation was noticed. The highest TRAP activity was found in 0.5 wt% Si doped brushite cements. Further increase in Si amount to 1.1 wt% reduced the osteoclast-like-cell numbers suggesting the inhibitory effect of dopant after specific level. In addition, new bone formation was enhanced in doped cements after 4 weeks. Although Si dopant did not affect the blood vessel formation at early time points, there was a significant increase after 8 weeks in 0.8 and 1.1 wt. % Si doped cements. Present results can be used to manipulate short and long term resorptive properties, as well as *in vivo* osteogenic and vasculogenic properties of brushite cement depending on the application requirement.

Supplementary Material

Refer to Web version on PubMed Central for supplementary material.

Acknowledgments

Authors acknowledge financial support from the National Institute of Health (N1H-R01-EB-007351) and NIH National Institute of Arthritis and Musculoskeletal and Skin Diseases (NIAMS, Grant No. 1R01AR066361). Authors thank Dr. Solaiman Tarafder and Franceschi Microscopy and Imaging Center, Washington State University for helpful assistance in the immunohistochemistry analysis and FESEM imaging.

References

1. Komath M, Varma HK. Development of a fully injectable calcium phosphate cement for orthopedic and dental applications. Bull Mater Sci. 2003; 26:415–22.
2. Hou C, Chen C, Hou S, Li Y, Lin F. The fabrication and characterization of dicalcium phosphate dihydrate-modified magnetic nanoparticles and their performance in hyperthermia processes in vitro. Biomaterials. 2009; 30:4700–7. [PubMed: 19501902]
3. Pina S, Vieira SI, Rego P, Torres PM, da Cruz e Silva OA, da Cruz e Silva EF, Ferreira JM. Biological responses of brushite-forming Zn- and ZnSr- substituted beta-tricalcium phosphate bone cements. Eur Cell Mater. 2010; 20:162–77. [PubMed: 20821372]

4. Brown, WE.; Chow, LC. A new calcium phosphate water setting cement. In: Brown, PW., editor. Cements research progress. Westerville, OH: Am. Ceram. Soc; 1986. p. 352-79.
5. Stadelmann VA, Bretton E, Terrier A, Procter P, Pioletti DP. Calcium phosphate cement augmentation of cancellous bone screws can compensate for the absence of cortical fixation. J Biomech. 2010; 43:2869–74. [PubMed: 20728888]
6. Ginebra M-P, Canal C, Espanol M, Pastorino D, Montufar EB. Calcium phosphate cements as drug delivery materials. Adv Drug Deliv Rev. 2012; 64:1090–1110. [PubMed: 22310160]
7. Xia Z, Grover LM, Huang Y, Adamopoulos IE, Gbureck U, Triffitt JT, Shelton RM, Barralet JE. In vitro biodegradation of three brushite calcium phosphate cements by a macrophage cell-line. Biomaterials. 2006; 27:4557–65. [PubMed: 16720039]
8. Grover LM, Hofmann MP, Gbureck U, Kumarasami B, Barralet JE. Frozen delivery of brushite calcium phosphate cements. Acta Biomater. 2008; 4:1916–23. [PubMed: 18657496]
9. Grover LM, Knowles JC, Fleming GJP, Barralet JE. In vitro ageing of brushite calcium phosphate cement. Biomaterials. 2003; 24:4133–41. [PubMed: 12853243]
10. Tas AC. Granules of Brushite and Octacalcium Phosphate from Marble. J Am Ceram Soc. 2011; 94:3722–6.
11. Huan Z, Chang J. Novel bioactive composite bone cements based on the β-tricalcium phosphate–monocalcium phosphate monohydrate composite cement system. Acta Biomater. 2009; 5:1253–64. [PubMed: 18996779]
12. Ogata H, Hayashi M, Tsuda H, Suzuki N, Maeno M, Sugawara A, Ogiso B. Effects of a calcium phosphate cement on mineralized nodule formation compared with endodontic cements. Dent Mater J. 2012; 31:92–7. [PubMed: 22277611]
13. Ramaswamy Y, Wu C, Van Hummel A, Combes V, Grau G, Zreiqat H. The responses of osteoblasts, osteoclasts and endothelial cells to zirconium modified calcium-silicate-based ceramic. Biomaterials. 2008; 29:4392–402. [PubMed: 18757093]
14. Schilling AF, Linhart W, Filke S, Gebauer M, Schinke T, Rueger JM, Amling M. Resorbability of bone substitute biomaterials by human osteoclasts. Biomaterials. 2004; 25:3963–72. [PubMed: 15046886]
15. Klammert U, Reuther T, Blank M, Reske I, Barralet JE, Grover LM, Kübler AC, Gbureck U. Phase composition, mechanical performance and in vitro biocompatibility of hydraulic setting calcium magnesium phosphate cement. Acta Biomater. 2010; 6:1529–35. [PubMed: 19837194]
16. Hoppe A, Güldal NS, Boccaccini AR. A review of the biological response to ionic dissolution products from bioactive glasses and glass-ceramics. Biomaterials. 2011; 32:2757–74. [PubMed: 21292319]
17. Beck GR Jr, Ha S-W, Camalier CE, Yamaguchi M, Li Y, Lee J-K, Weitzmann MN. Bioactive silica-based nanoparticles stimulate bone-forming osteoblasts, suppress bone-resorbing osteoclasts, and enhance bone mineral density in vivo. Nanomedicine. 2012; 8:793–803. [PubMed: 22100753]
18. Hing KA, Revell PA, Smith N, Buckland T. Effect of silicon level on rate, quality and progression of bone healing within silicate-substituted porous hydroxyapatite scaffolds. Biomaterials. 2006; 27:5014–26. [PubMed: 16790272]
19. Pietak AM, Reid JW, Stott MJ, Sayer M. Silicon substitution in the calcium phosphate bioceramics. Biomaterials. 2007; 28:4023–32. [PubMed: 17544500]
20. Roy M, Fielding GA, Bandyopadhyay A, Bose S. Effects of zinc and strontium substitution in tricalcium phosphate on osteoclast differentiation and resorption. Biomater Sci. 2012; 1:74–82.
21. Roy M, Bose S. Osteoclastogenesis and osteoclastic resorption of tricalcium phosphate: Effect of strontium and magnesium doping. J Biomed Mater Res A. 2012; 100A:2450–61. [PubMed: 22566212]
22. Botelho CM, Brooks RA, Spence G, McFarlane I, Lopes MA, Best SM, Santos JD, Rushton N, Bonfield W. Differentiation of mononuclear precursors into osteoclasts on the surface of Si-substituted hydroxyapatite. J Biomed Mater Res A. 2006; 78A:709–20. [PubMed: 16739170]
23. Carmeliet P. Angiogenesis in health and disease. Nat Med. 2003; 9:653–60. [PubMed: 12778163]

24. Vincent C, Kogawa M, Findlay DM, Atkins GJ. The generation of osteoclasts from RAW 264.7 precursors in defined, serum-free conditions. J Bone Miner Metab. 2009; 27:114–9. [PubMed: 19057837]
25. Roy M, DeVoe K, Bandyopadhyay A, Bose S. Mechanical property and in vitro biocompatibility of brushite cement modified by polyethylene glycol. Mater Sci Eng C. 2012; 32:2145–52.
26. Bohner M, Theiss F, Apelt D, Hirsiger W, Houriet R, Rizzoli G, Gnos E, Frei C, Auer JA, von Rechenberg B. Compositional changes of a dicalcium phosphate dihydrate cement after implantation in sheep. Biomaterials. 2003; 24:3463–74. [PubMed: 12809775]
27. Bohner M, Lemaitre J, Ring TA. Effects of Sulfate, Pyrophosphate, and Citrate Ions on the Physicochemical Properties of Cements Made of β-Tricalcium Phosphate-Phosphoric Acid-Water Mixtures. J Am Ceram Soc. 1996; 79:1427–34.
28. Tamimi F, Sheikh Z, Barralet J. Dicalcium phosphate cements: Brushite and monetite. Acta Biomater. 2012; 8:474–487. [PubMed: 21856456]
29. Bohner M. Reactivity of calcium phosphate cements. J Mater Chem. 2007; 17:3980–3986.
30. Langstaff S, Sayer M, Smith TJ, Pugh SM. Resorbable bioceramics based on stabilized calcium phosphates. Part II: evaluation of biological response. Biomaterials. 2001; 22:135–50. [PubMed: 11101158]
31. Bandyopadhyay A, Bernard S, Xue W, Bose S. Calcium Phosphate-Based Resorbable Ceramics: Influence of MgO, ZnO, and SiO2 Dopants. J Am Ceram Soc. 2006; 89:2675–88.
32. Hofmann MP, Mohammed AR, Perrie Y, Gbureck U, Barralet JE. High-strength resorbable brushite bone cement with controlled drug-releasing capabilities. Acta Biomater. 2009; 5:43–9. [PubMed: 18799378]
33. Lehmann G, Cacciotti I, Palmero P, Montanaro L, Bianco A, Campagnolo L, Camaioni A. Differentiation of osteoblast and osteoclast precursors on pure and silicon-substituted synthesized hydroxyapatites. Biomed Mater. 2012; 7:055001. [PubMed: 22781924]
34. Jokic B, Mitric M, Popovic M, Sima L, Petrescu SM, Petrovic R, Janackovic Dj. The influence of silicon substitution on the properties of spherical- and whisker-like biphasic α-calcium-phosphate/hydroxyapatite particles. J Mater Sci Mater Med. 2011; 22:2175–85. [PubMed: 21823030]
35. Alkhraisat MH, Mariño FT, Retama JR, Jerez LB, López-Cabarcos E. Beta-tricalcium phosphate release from brushite cement surface. J Biomed Mater Res A. 2008; 84A:710–7. [PubMed: 17635024]
36. Grover LM, Gbureck U, Wright AJ, Tremayne M, Barralet JE. Biologically mediated resorption of brushite cement in vitro. Biomaterials. 2006; 27:2178–85. [PubMed: 16337265]
37. Hing KA, Revell PA, Smith N, Buckland T. Effect of silicon level on rate, quality and progression of bone healing within silicate-substituted porous hydroxyapatite scaffolds. Biomaterials. 2006; 27:5014–5026. [PubMed: 16790272]
38. Jones JR, Tsigkou O, Coates EE, Stevens MM, Polak JM, Hench LL. Extracellular matrix formation and mineralization on a phosphate-free porous bioactive glass scaffold using primary human osteoblast (HOB) cells. Biomaterials. 2007; 28:1653–1663. [PubMed: 17175022]
39. Obata Q, Kasugav T. Stimulation of human mesenchymal stem cells and osteoblasts activities *in vitro* on silicon-releasable scaffolds. J Biomed Mater Res A. 2009; 91:11–17. [PubMed: 18683233]
40. Reffitt D, Ogston N, Jugdaohsingh R, Cheung HF, Evans BA, Thompson RP, Powell JJ, Hampson GN. Orthosilicic acid stimulates collagen type 1 synthesis and osteoblastic differentiation in human osteoblast-like cells in vitro. Bone. 2003; 32:127–135. [PubMed: 12633784]
41. Li H, Chang J. Bioactive silicate materials stimulate angiogenesis in fibroblast and endothelial cell co-culture system through paracrine effect. Acta Biomater. 2013; 9:6981–6991. [PubMed: 23416471]
42. Saghiri, MA.; Asatourian, A.; Orangi, J.; Sorenson, CM.; Sheibani, N. Functional role of inorganic trace elements in angiogenesis—Part II: Cr,Si, Zn, Cu, and S. Crit Rev Oncol Hematol. 2015. DOI: http://dx.doi.org/10.1016/j.critrevonc.2015.05.011
43. Stähli C, James-Bhasin M, Hoppe A, Boccaccini AR, Nazhat SN. Effect of ion release from Cu-doped 45S5 Bioglass® on 3D endothelial cell Morphogenesis. Acta Biomater. 2015; 19:15–22. [PubMed: 25770928]

44. El-Gendy R, Kirkham J, Newby PJ, Mohanram Y, Boccaccini AR, Yang XB. Investigating the Vascularization of Tissue-Engineered Bone Constructs Using Dental Pulp Cells and 45S5 Bioglass® Scaffolds. Tissue Eng Part A. 2015; 2110.1089/ten.tea.2014.0485

45. Kong N, Lin K, Li H, Chang J. Synergy effects of copper and silicon ions on stimulation of vascularization by copper-doped calcium silicate. J Mater Chem B. 2014; 2:1100–1110.

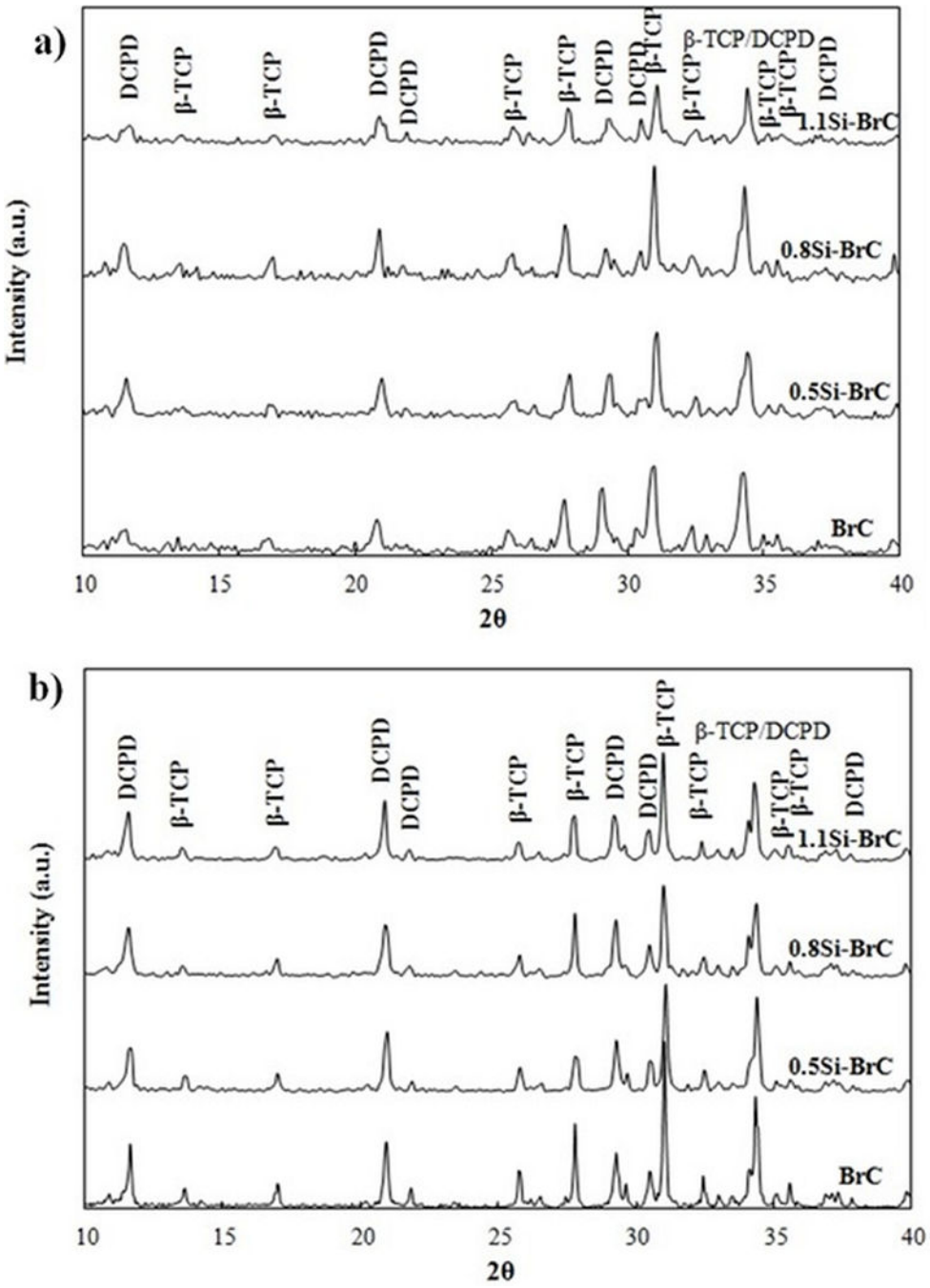

Figure 1.

XRD pattern of BrC samples after a) 1 day of immersion in PBS, and b) 14 days of immersion in non-cell supplemented DMEM.

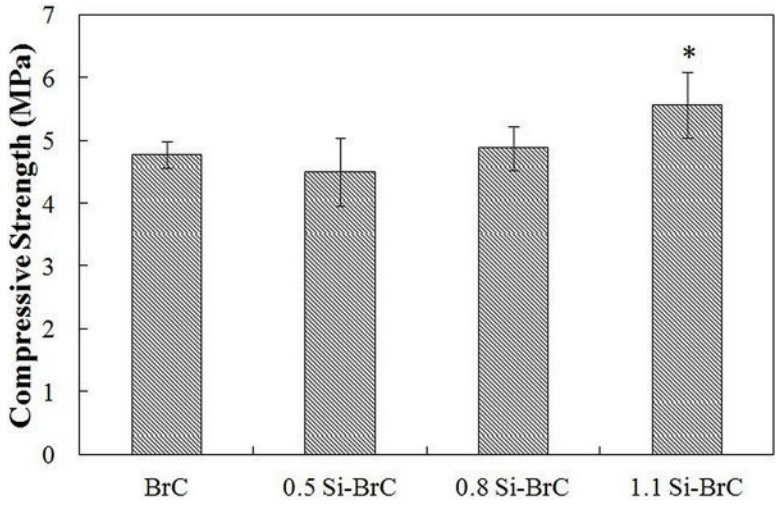

Figure 2.
Compressive strength of BrC samples after 1 day of immersion in PBS.

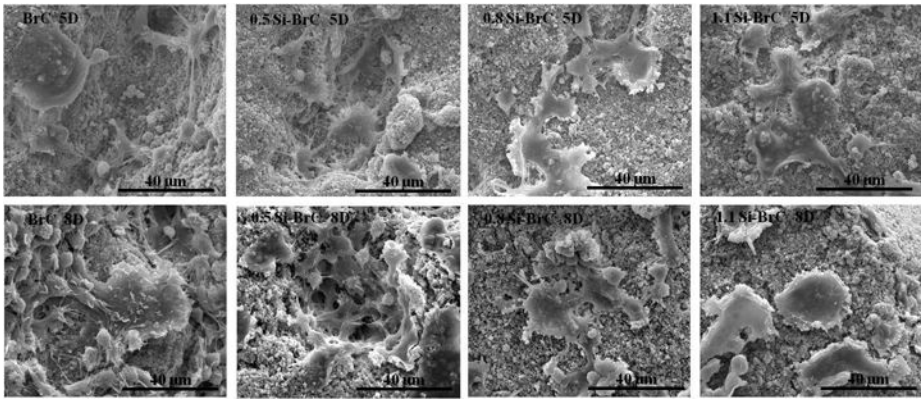

Figure 3.
Osteoclast cell morphology on undoped and Si-doped brushite cements after 5 and 8 days of culture.

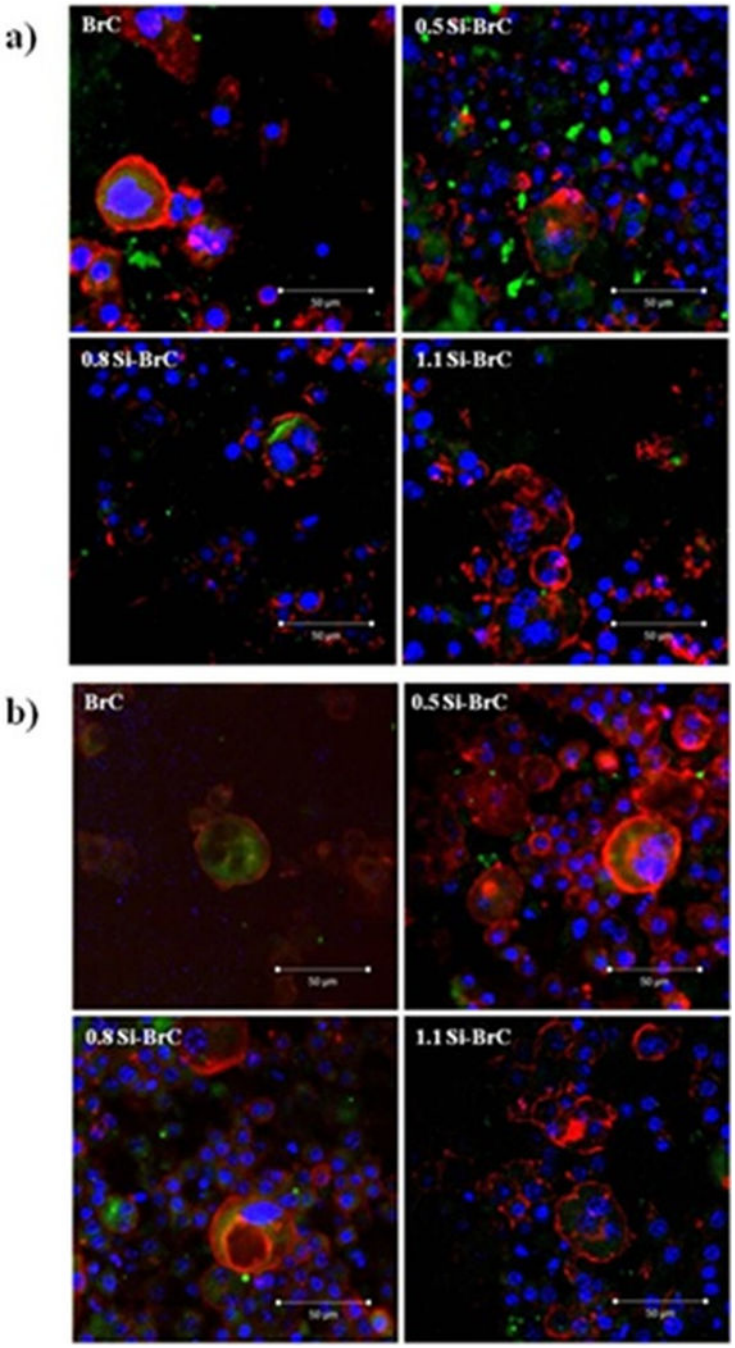

Figure 4.
Fluorescence microscopy showing actin ring (red), cell nuclei (blue), and vitronectin receptor $\alpha_v\beta_3$ integrin (green) after a) 8 days and b) 14 days of culture.

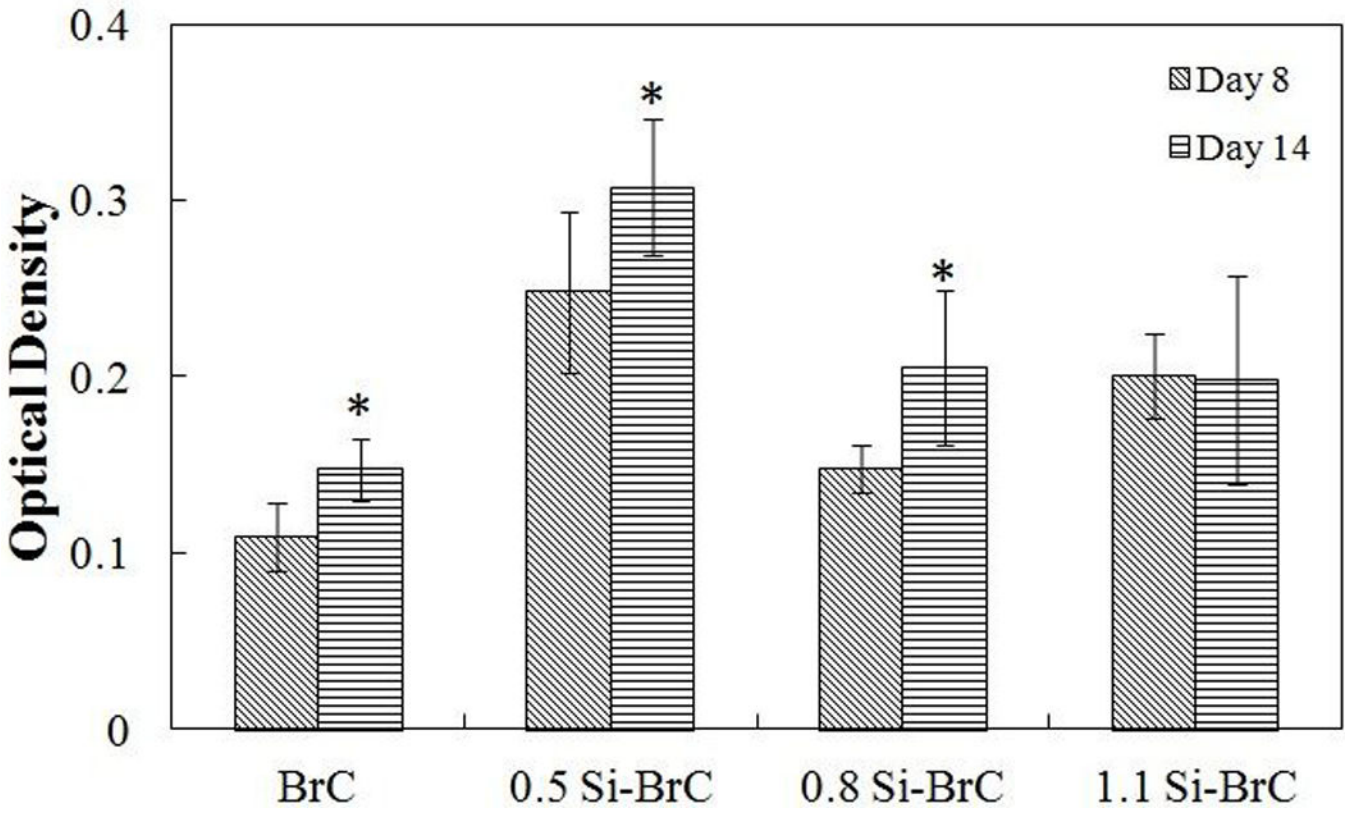

Figure 5.
TRAP assay as a function of composition and culture day.

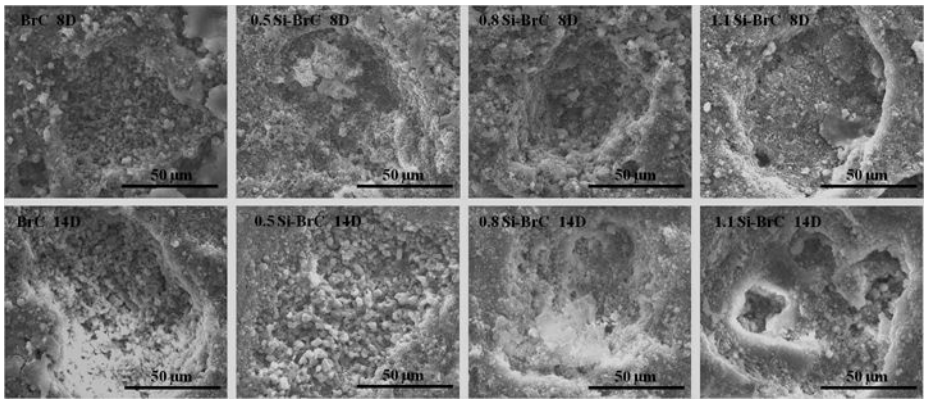

Figure 6.
Surface morphology of cement samples after culturing with RAW 264.7 cells.

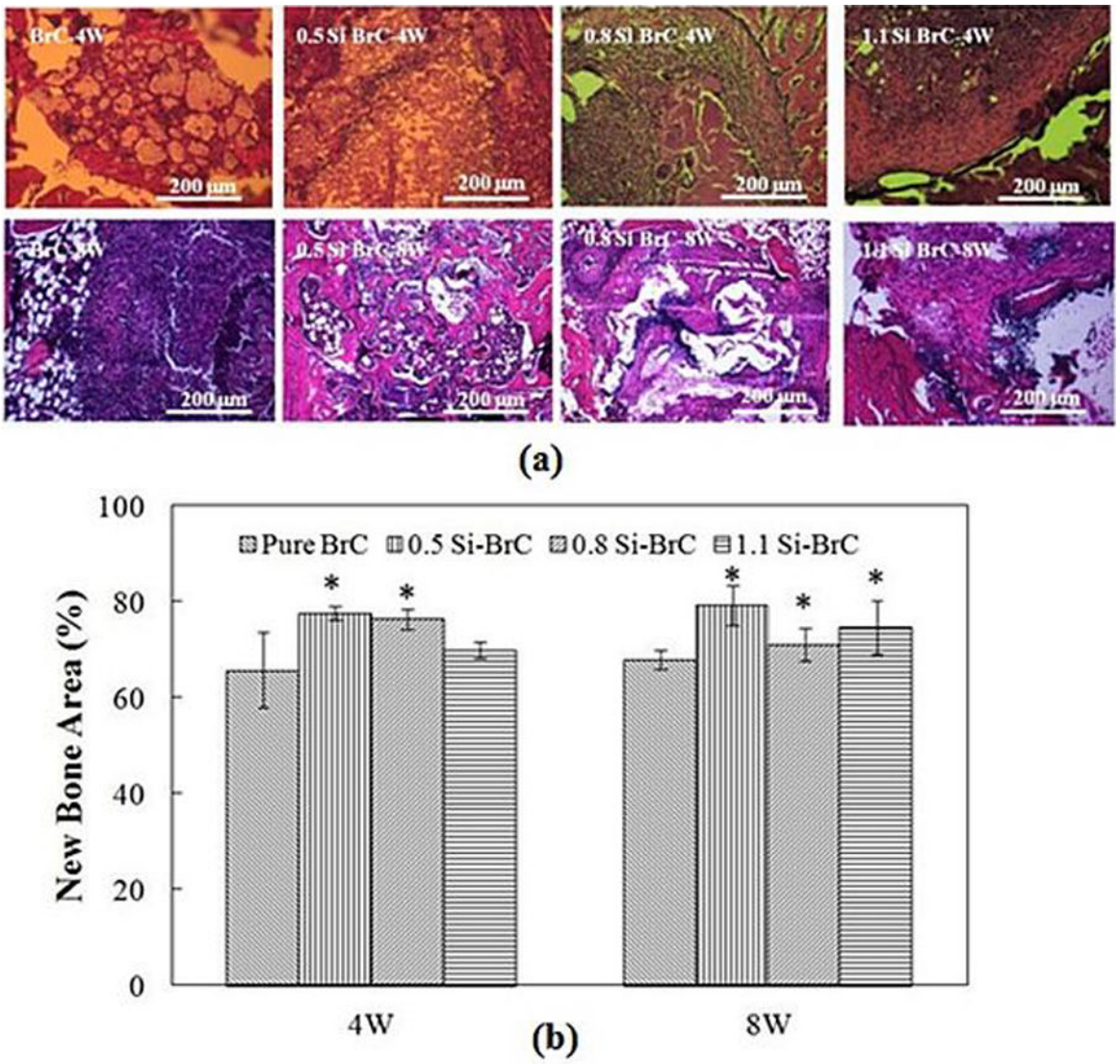

Figure 7.

a) Photomicrographs of representative histological sections after hematoxylin and eosin (H&E) staining of decalcified tissue sections showing the development of bone formation after 4 & 8 weeks. Black = Bone marrow; Pink/Reddish = New/old bone; Yellowish/Whitish = acellular regions derive from scaffold, b) Histomorphometric analysis of bone area fraction (total newly formed bone area/total area, %).

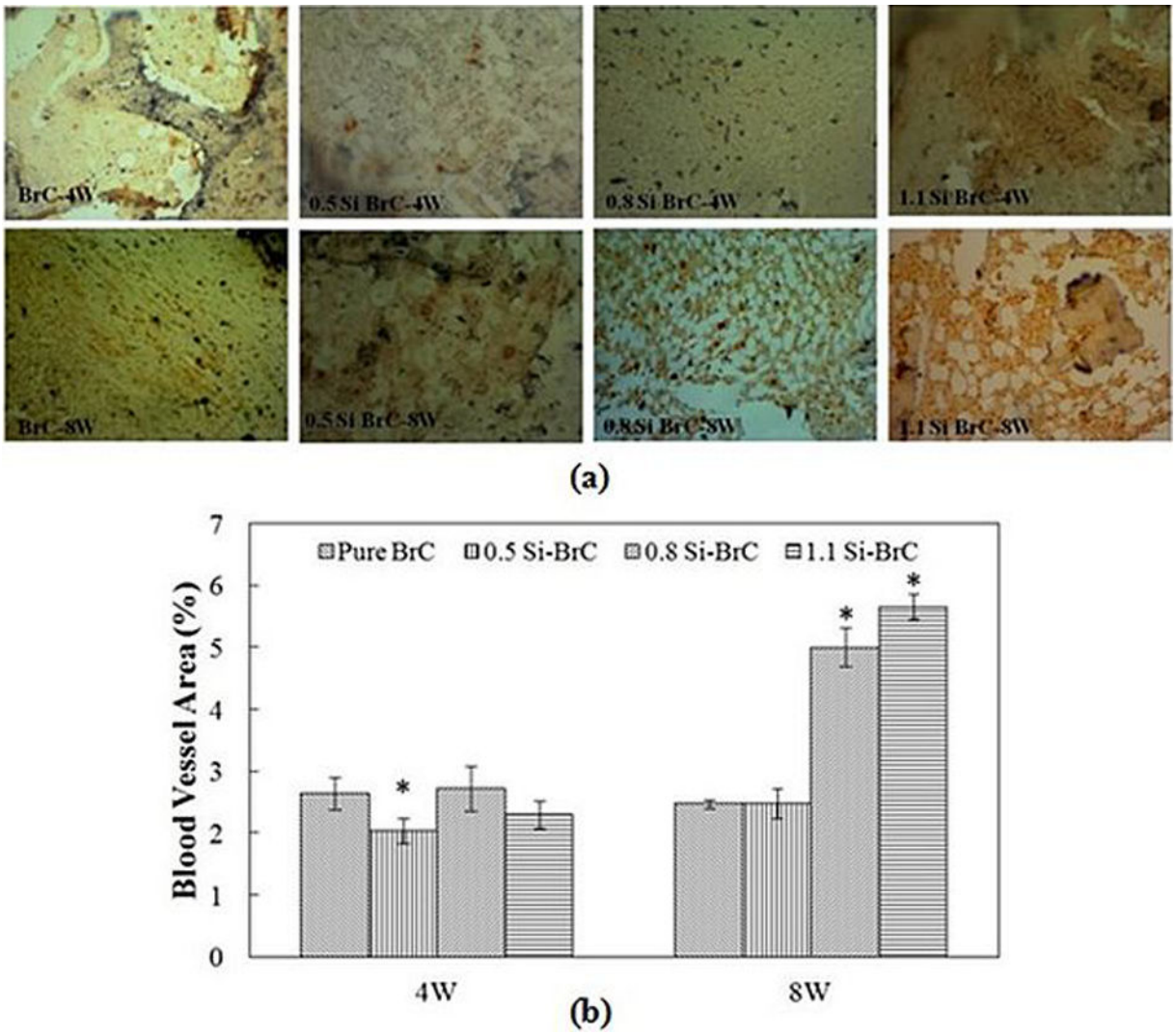

Figure 8.

a) Photomicrograph of vWF stained tissue sections showing blood vessel formation after 4 and 8 weeks in BrCs. vWF positive signals are brown/red with hematoxylin counterstaining, b) Histomorphometric analysis showing new blood vessel area comparisons between undoped and Si doped BrC (vWF positive area/total area, %).

Table 1

Physical properties of undoped and doped brushite cements.

Composition	Initial setting time (min)	Final setting time (min)	β-TCP/DCPD before immersion	β-TCP/DCPD after immersion
BrC	5	11	1.81	2.44
0.5 Si- BrC	3.5	12	1.81	2.12
0.8 Si- BrC	4	11	1.72	2.17
1.1 Si- BrC	4	19	1.79	2.04